

# **PERMIAN-TRIASSIC STABLE ISOTOPE STRATIGRAPHY OF AUSTRALIA**

Thesis submitted as a requirement of the  
Doctor of Philosophy degree,  
Macquarie University,  
New South Wales

**Richard Morante M.Sc., B.Sc., Dip.T.Sc.**

September, 1995



# MACQUARIE UNIVERSITY

## HIGHER DEGREE THESIS AUTHOR'S CONSENT (DOCTORAL)

This is to certify that I, R. MORANTE  
being a candidate for the degree of Doctor of PHILOSOPHY  
am aware of the policy of the University relating to the retention and use  
of higher degree theses as contained in the University's Doctoral Rules  
generally, and in particular Rule 7(7).

In the light of this policy and the policy of the above Rules, I agree to allow  
a copy of my thesis to be deposited in the University Library for consultation,  
loan and photocopying forthwith.

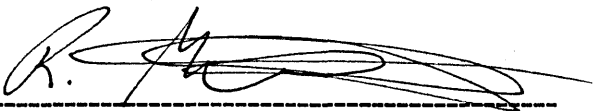
J. J. Hewson  
Signature of Witness

R. Morante  
Signature of Candidate

Dated this 27th day of September 1995

The Academic Senate on 21 February '96 resolved that the candidate  
had satisfied requirements for admission to the degree of PhD.  
This thesis represents a major part of the prescribed program of study.

I hereby certify that the work embodied in this thesis is the result of original research and has not been submitted for a higher degree to any other University or Institution



A handwritten signature in black ink, appearing to be 'R. Morante', is written over a horizontal dashed line.

### ***Acknowledgements***

Supported by an ARC Special Investigator Award to J.J Veevers and a Macquarie University Postgraduate Award to R. Morante. Analyses were conducted at the Centre for Isotope Studies (CIS). R. Helby and P. Price provided Paradise core samples from Inland Exploration N.L. D. Grybowski of SANTOS provided samples from Tern-3. B. Messent of BHP Petroleum provided samples from Fishburn-1. Samples from the Bowen Basin were obtained from the GSQ and UQ collections. D. Gravestock of SADME provided samples from Merrimelia-3. J.M. Dickins (AGSO) provided samples from outcrop in the Canning Basin. D. Briggs (U.N.S.W) provided outcrop samples from the Sydney and Bowen Basins. J.D. Campbell (University of Otago) and J.I. Raine (DSIR) provided samples from Southland, New Zealand. D. Cole (GSSA) provided samples from South Africa. A. Todd (CIS), S. Craven, A. Bryce, and J. Trotter (CSIRO) assisted with isotope sample analysis techniques. K. Riley assisted with H/C analyses. C. Herbert (Macquarie University) and G. Retallack (University of Oregon) discussed environmental aspects and sedimentology of cores. In New Zealand J.D. Campbell guided me in the field. J. Roberts (U.N.S.W.) provided radiometric dates ahead of publication. I thank N. Archbold (Deakin University), J. Backhouse (WAGS), D. Briggs (UNSW), C. Foster (AGSO), J. Hamilton (CSIRO), R. Helby, V. Palmieri (GSQ), M. Smyth (CSIRO), M. Walter (MU), and G. Woods (SANTOS) for discussion. I am deeply indebted to R. Helby for providing fresh palynological determinations. A. Andrew, P. Schmidt, J. Veevers, and D. Whitford provided guidance and supervision.

I thank Vicki and Kiah for their support during this study.

# TABLE OF CONTENTS

	Page no
ABSTRACT	1
1. INTRODUCTION	
1.0 The Permian-Triassic boundary	3
1.1 The Permian-Triassic boundary in Australia	4
1.2 Project development	7
1.3 Isotope chemostratigraphy	7
1.4 Negative shifts in global $\delta^{13}\text{C}_{\text{CO}_3}$ and $\delta^{13}\text{C}_{\text{org}}$	10
1.5 $\delta^{13}\text{C}_{\text{CO}_3}$ about the Permian-Triassic boundary	11
1.6 $\delta^{13}\text{C}_{\text{org}}$ across the Permian-Triassic boundary outside of Australia- previous work	18
1.7 The nonmarine $\delta^{13}\text{C}_{\text{CO}_3}$ record- previous work	19
1.8 Analysis of $\delta^{13}\text{C}$ profiles	19
1.9 $\delta^{13}\text{C}$ reference section	20
2. AUSTRALIAN $\delta^{13}\text{C}_{\text{org}}$ -ISOTOPE PROFILES ABOUT THE PERMIAN-TRIASSIC (P/TR) BOUNDARY.	23
2.1 Bonaparte Basin	26
2.1.1 Tern-3	28
2.1.2 Petrel-4	30
2.1.3 Fishburn-1	34
2.1.4 Sahul Shoals-1	38
2.1.5 Bonaparte Basin synopsis	40
2.2 Canning Basin	42
2.2.1 Paradise Cores	42
2.3 The Carnarvon Basin	51
2.3.1 Onslow-1	51
2.4 Perth Basin	54
2.4.1 Whicher Range-1	55
2.4.2 BMR-10 (Beagle Ridge)	57
2.5 Bowen Basin	59
2.5.1 Denison NS20	61
2.5.2 GSQ Eddystone 1	64
2.5.3 GSQ Eddystone 5	64
2.5.4 GSQ Taroom-10	64
2.5.5 Bowen Basin synopsis	73
2.6 Sydney Basin	74
2.6.1 DM Murrays Run-1	75
2.6.2 Bunnerong DDH 1	79
2.6.3 Lisarow DDH 1	80

2.6.4 Awaba DDH 2	83
2.6.5 DM Newvale DDH 28	86
2.6.6 Sydney Basin synopsis	88
2.7 Cooper Basin	90
2.7.1. Merrimelia-3	91
2.8 Synopsis of all Australian $\delta^{13}\text{C}_{\text{org}}$ data	95
APPENDIX 2.1	
$\delta^{13}\text{C}_{\text{org}}$ profiles about the Permian-Triassic boundary? from New Zealand and South Africa	96
New Zealand; G46, Popotonoa Fm	96
South Africa; SW1/67, Karoo Basin	98
APPENDIX 2.2:	
Organic carbon analysis techniques	101
APPENDIX 2.3	
Isotopic analysis of Sm/Nd (samarium/neodymium)	104
 3 STRONTIUM ISOTOPE SEAWATER CURVE IN THE LATE PERMIAN OF AUSTRALIA.	 105
3.1 Introduction	106
3.2 Sample selection	106
3.3 Method	107
3.4 Results	108
3.5 Discussion	112
3.6 Conclusions	112
APPENDIX 3.1	
Strontium isotope analysis techniques	114
APPENDIX 3.2	
Calcite isotopic analyses	116
APPENDIX 3.3	
Cathode luminescence microscopy	117
 4 $\delta^{13}\text{C}_{\text{CO}_3}$ AND $\delta^{18}\text{O}_{\text{CO}_3}$ SEAWATER PROFILES THROUGH THE PERMIAN-TRIASSIC OF AUSTRALASIA	 119
4.1 Introduction	119
4.2 Sample selection and screening	119
4.3 Results and discussion	120
4.4 Conclusions	127
4.5 Palaeotemperature estimates from the Permian Panthalassan margin sediments of Eastern Australia	128
4.6 Results	129
4.7 Conclusions	129
APPENDIX 4.1	131
Location of outcrop samples analysed for carbon and oxygen stable isotopes.	131

## 5. PALEOMAGNETIC STRATIGRAPHY ABOUT THE PERMIAN/TRIASSIC BOUNDARY IN AUSTRALIA

5.1 Paleomagnetism in the Merrimelia-3 borehole, Cooper Basin	132
5.2 Methods	132
5.3 Results	132
5.4 Discussion	136
5.5 Conclusions	136

## 6. SYNTHESIS

6.1. Carbon isotope results: Summary	139
6.2 Implications of the $\delta^{13}\text{C}_{\text{org}}$ profiles for the Permian-Triassic timescale in Australia	142
6.3 Mass and $\delta^{13}\text{C}$ balance constraints for the Permian and Early Triassic	142
6.4 Interpretation of $\delta^{13}\text{C}$ isotope profiles	144
6.5 The Permian-Triassic $\delta^{13}\text{C}$ excursion - implications for the flux rates of carbon between reduced and oxidised reservoirs	146
6.6 $^{87}\text{Sr}/^{86}\text{Sr}$ results summary and interpretation	147
6.7 Implications for the Australian Permian timescale	148
6.8 Synopsis	149
6.9 A model for the cause of the Permian-Triassic mass extinction	150
6.10 Permian and Triassic timescales in Australia	157
6.11 Composite profiles of $\delta^{13}\text{C}_{\text{org}}$ , $\delta^{13}\text{C}_{\text{CO}_3}$ , $\Delta$ , $\delta^{18}\text{O}_{\text{CO}_3}$ , and $^{87}\text{Sr}/^{86}\text{Sr}$ through the Permian -Triassic	163
6.12 Conclusion	164

REFERENCES CITED	171
------------------	-----

## APPENDIX

Publications and conference abstracts reporting progress during this project.

1. not available.

2.- 10. supplied

183

## LIST OF FIGURES

### CHAPTER 1

Fig. 1.1 Nammal Gorge, Salt Range, Pakistan, showing formations, zones, and $\delta^{13}\text{C}_{\text{CO}_3}$ .	6
Fig. 1.2 Secular isotopic age curves for strontium, carbon, sulfur, and oxygen.	8
Fig. 1.3 Variation of $\delta^{13}\text{C}_{\text{CO}_3}$ and $\delta^{13}\text{C}_{\text{org}}$ as a function of the % of carbon buried as organic carbon.	10
Fig. 1.4 $\delta^{13}\text{C}_{\text{CO}_3}$ profiles from Austria, Yugoslavia, southwestern Turkey, northwestern Iran, northern Iran, Pakistan, and China (Zhejaing, Shangsi and Guizhou) about the Permian-Triassic datum.	13
Fig. 1.5 Locations shown on Fig. 1.4 and of Australian sections studied.	
Fig. 1.6 Meishan Section D, China $\delta^{13}\text{C}_{\text{CO}_3}$ profile, lithology and formations.	16
Fig. 1.7 Gartnerkofel-1, Austria, $\delta^{13}\text{C}_{\text{org}}$ , $\delta^{13}\text{C}_{\text{CO}_3}$ , lithology, and formations.	17
Fig. 1.8 $\delta^{13}\text{C}_{\text{org}}$ from the Permian-Triassic boundary at Williston Lake, British Columbia.	18
Fig. 1.9 $\delta^{13}\text{C}$ profiles divided into segments A-D across the Permian-Triassic boundary.	19

### CHAPTER 2

Fig. 2.0 Location of Australian sedimentary basins sampled.	24
Fig. 2.1 Equivalence of palynological zonation schemes.	25
Fig. 2.2 Location of Tern-3, Petrel-1, Fishburn-1, and Sahul Shoals-1.	27
Fig. 2.3 Tern-3 total organic carbon (TOC), $\delta^{13}\text{C}_{\text{org}}$ , palynological zones, lithological log, and formations.	29
Fig. 2.4 Petrel-4 total organic carbon (TOC), $\delta^{13}\text{C}_{\text{org}}$ , palynological zones, lithological log, and formations.	32
Fig. 2.5 Petrel-4, alternative interpretation.	33
Fig. 2.6 Fishburn-1 total organic carbon (TOC), $\delta^{13}\text{C}_{\text{org}}$ , palynological zones, lithological log, and formations.	37
Fig. 2.7 Sahul Shoals-1 total organic carbon (TOC), $\delta^{13}\text{C}_{\text{org}}$ , palynological zones, dinoflagellate zones, conodont zones, lithological log, and formations.	39
Fig. 2.8 Bonaparte Basin $\delta^{13}\text{C}_{\text{org}}$ profiles aligned on the beginning of the $\delta^{13}\text{C}_{\text{org}}$ excursion.	41
Fig. 2.9 Location of the Paradise Coreholes.	44
Fig. 2.10 Composite section of Paradise core-holes 1-6, total organic carbon (TOC), $\delta^{13}\text{C}_{\text{org}}$ , palynological zones, lithological log, and formations.	49
Fig. 2.11 Paradise core-hole 4 total organic carbon (TOC), $\delta^{13}\text{C}_{\text{org}}$ .	50
Fig. 2.12 Location of Onslow-1.	52
Fig. 2.13 Onslow-1 total organic carbon (TOC), $\delta^{13}\text{C}_{\text{org}}$ , palynological zones, lithological log, and formations.	53
Fig. 2.14 Location of BMR-10 (Beagle Ridge) and Whicher Range-1.	54
Fig. 2.15 Whicher Range-1, total organic carbon (TOC), $\delta^{13}\text{C}_{\text{org}}$ , palynological zones, lithological log, and formations.	56



Fig. 2.16 BMR-10 (Beagle Ridge), total organic carbon (TOC), $\delta^{13}\text{C}_{\text{org}}$ , palynological zones, lithological log, and formations.	58
Fig. 2.17 Location of Denison NS 20, Eddystone 1, Eddystone 5, Taroom 10 and Springsure-19.	59
Fig. 2.18 Generalised stratigraphy of the Denison Trough, Bowen Basin.	60
Fig.2.19 Denison NS 20, total organic carbon (TOC), $\delta^{13}\text{C}_{\text{org}}$ , palynological zones, lithological log, and formations.	63
Fig. 2.20 Eddystone-1, total organic carbon (TOC), $\delta^{13}\text{C}_{\text{org}}$ , $\delta^{13}\text{C}_{\text{CO}_3}$ , $\delta^{18}\text{O}_{\text{CO}_3}$ , $^{87}\text{Sr}/^{86}\text{Sr}$ , palynological zones, foraminifera zones, brachiopod zones, lithological log, and formations.	67
Fig. 2.21 TOC vs $\delta^{13}\text{C}_{\text{org}}$ of the samples from the lower Rewan Formation in Eddystone-1.	68
Fig 2.22 Eddystone-5, total organic carbon (TOC), $\delta^{13}\text{C}_{\text{org}}$ , $\delta^{13}\text{C}_{\text{CO}_3}$ , $\delta^{18}\text{O}_{\text{CO}_3}$ , $^{87}\text{Sr}/^{86}\text{Sr}_{\text{CO}_3}$ , palynological zones, the top of the Reids Dome Beds are Stage 3b, foraminiferan zones, brachiopod zones, lithological log, and formations.	70
Fig. 2.23 Taroom-10, total organic carbon (TOC), $\delta^{13}\text{C}_{\text{org}}$ , $\delta^{13}\text{C}_{\text{CO}_3}$ , $\delta^{18}\text{O}_{\text{CO}_3}$ , $^{87}\text{Sr}/^{86}\text{Sr}_{\text{CO}_3}$ , palynological zones, foraminifera zones, brachiopod zones, lithological log and formations.	72
Fig. 2.24 Location of Murrays Run DDH 1, Awaba DDH 2, Bunnerong DDH 1, Lisarow DDH 1, and Newvale DDH 28.	74
Fig. 2.25 Murrays Run DDH 1, total organic carbon (TOC) and $\delta^{13}\text{C}_{\text{org}}$ (expanded about the negative excursion, palynological zones, lithological log, and formations.	78
Fig. 2.26 Bunnerong DDH 1, total organic carbon (TOC), $\delta^{13}\text{C}_{\text{org}}$ , palynological zones, lithological log, and formations.	79
Fig 2.27 Lisarow DDH 1, total organic carbon (TOC), $\delta^{13}\text{C}_{\text{org}}$ , palynological zones, lithological log, formations.	81
Fig. 2.28 TOC vs $\delta^{13}\text{C}_{\text{org}}$ for the lower Narrabeen Group samples in Lisarow-1.	82
Fig. 2.29 Awaba DDH 2, total organic carbon (TOC), $\delta^{13}\text{C}_{\text{org}}$ , palynological zones, lithological log, and formations.	85
Fig. 2.30 Newvale DDH 28, total organic carbon (TOC), $\delta^{13}\text{C}_{\text{org}}$ , palynological zones, lithological log, and formations.	87
Fig. 2.31 Sydney Basin $\delta^{13}\text{C}_{\text{org}}$ profiles aligned at the Coal Measures/Narrabeen Group lithostratigraphic boundary.	89
Fig. 2.32 Location of Merrimelia-3.	90
Fig. 2.33 Merrimelia-3, magnetic polarity, total organic carbon (TOC), $\delta^{13}\text{C}_{\text{org}}$ , palynological zones, lithological log, and formations.	94
Fig. 2.34 Location of the Popotonoa section, Southland.	96
Fig. 2.35 Popotonoa Fm: $\delta^{13}\text{C}_{\text{org}}$ , TOC, lithology and stratigraphy.	97
Fig. 2.36 SW 1/67, Karoo Basin, South Africa. TOC, $\delta^{13}\text{C}_{\text{org}}$ , palynological zones, lithological log, and formations.	100
Fig. 2.37 Organic carbon processing technique.	101
Fig. 2.38 $\delta^{13}\text{C}_{\text{org}}$ of the standard CSIRO anthracite samples processed with rock samples in this study.	103

## CHAPTER 3

- Fig. 3.1  $^{87}\text{Sr}/^{86}\text{Sr}$  seawater curve for the Mississippian- Triassic after Denison et al. (1994). Figs 4.1 Eddystone-1 total organic carbon (TOC),  $\delta^{13}\text{C}_{\text{org}}$ ,  $\delta^{13}\text{C}_{\text{CO}_3}$ ,  $\delta^{18}\text{O}_{\text{CO}_3}$ ,  $^{87}\text{Sr}/^{86}\text{Sr}$ , palynological zones, foraminifera zones, brachiopod zones, lithological log, and formations. 105
- Fig. 3.2 Eddystone-1, total organic carbon (TOC),  $\delta^{13}\text{C}_{\text{org}}$ ,  $\delta^{13}\text{C}_{\text{CO}_3}$ ,  $\delta^{18}\text{O}_{\text{CO}_3}$ ,  $^{87}\text{Sr}/^{86}\text{Sr}$ , palynological zones, and formations. 108
- Fig. 3.3 Eddystone-5, total organic carbon (TOC),  $\delta^{13}\text{C}_{\text{org}}$ ,  $\delta^{13}\text{C}_{\text{CO}_3}$ ,  $\delta^{18}\text{O}_{\text{CO}_3}$ ,  $^{87}\text{Sr}/^{86}\text{Sr}$ , palynological zones, and formations. 109
- Fig. 3.4 Taroom-10, total organic carbon (TOC),  $\delta^{13}\text{C}_{\text{org}}$ ,  $\delta^{13}\text{C}_{\text{CO}_3}$ ,  $\delta^{18}\text{O}_{\text{CO}_3}$ ,  $^{87}\text{Sr}/^{86}\text{Sr}$ , palynological zones, and formations. 110
- Fig.3.5 Plane polarised light and C.L. micrographs of a fabric retentive nonluminescent brachiopod. 118

## CHAPTER 4

- Fig. 4.1 Eddystone-1 total organic carbon (TOC),  $\delta^{13}\text{C}_{\text{org}}$ ,  $\delta^{13}\text{C}_{\text{CO}_3}$ ,  $\delta^{18}\text{O}_{\text{CO}_3}$ ,  $^{87}\text{Sr}/^{86}\text{Sr}$ , palynological zones, foraminifera zones, brachiopod zones, lithological log, and formations. 123
- Fig. 4.2 Eddystone-5 total organic carbon (TOC),  $\delta^{13}\text{C}_{\text{org}}$ ,  $\delta^{13}\text{C}_{\text{CO}_3}$ ,  $\delta^{18}\text{O}_{\text{CO}_3}$ ,  $^{87}\text{Sr}/^{86}\text{Sr}$ , palynological zones, foraminifera zones, brachiopod zones, lithological log, and formations. 124
- Fig. 4.3 Taroom-10 total organic carbon (TOC),  $\delta^{13}\text{C}_{\text{org}}$ ,  $\delta^{13}\text{C}_{\text{CO}_3}$ ,  $\delta^{18}\text{O}_{\text{CO}_3}$ ,  $^{87}\text{Sr}/^{86}\text{Sr}$ , palynological zones, foraminifera zones, brachiopod zones, lithological log, and formations. 125
- Fig. 4.4  $\delta^{18}\text{O}_{\text{CO}_3}$  vs  $\delta^{13}\text{C}_{\text{CO}_3}$  for non-luminescent Permian and Triassic brachiopod shells. 126
- Fig.4.5  $\delta^{18}\text{O}_{\text{CO}_3}$  vs  $\Delta$  for non-luminescent brachiopods from the Bowen Basin. 127

## CHAPTER 5

- Fig 5.1 Merrimelia-3, magnetic polarity, total organic carbon (TOC),  $\delta^{13}\text{C}_{\text{org}}$ , palynological zones, lithological log, and formations. 134
- Fig. 5.2 Intensity plot, stereographic and orthoganol plot of thermal and AF demagnetisation of selected specimens from above and below the negative  $\delta^{13}\text{C}_{\text{org}}$  excursion. 135
- Fig. 5.3 Magnetic polarity about the Permian-Triassic boundary at Shangsi. 137
- Fig. 5.4 Magnetic polarity profile about the Permian-Triassic boundary in Gartnerkofel-1 core. 138

## CHAPTER 6

- Fig. 6.1 Interpretation of carbon isotope profile segments. 145

Fig. 6.2 A is a modified Kvenvolden (1993) model showing how methane storage and release from clathrates moderates climate when eustatic level is controlled by glaciation but fails B when eustatic level is controlled by tectonics and leads to uncontrolled methane release.	153
Fig. 6.3 Permian-Triassic mass extinction cause hypothesis from Erwin (1993, fig. 9.4).	154
Fig. 6.4 The Australian Permian timescale.	161
Fig. 6.5 The Australian Permian and Triassic timescale.	162
Fig. 6.6 $\delta^{13}\text{C}_{\text{org}}$ profile through the Permian-Triassic.	165
Fig. 6.7 $\delta^{13}\text{C}_{\text{CO}_3}$ profile through the Permian-Triassic.	166
Fig. 6.8 $\Delta$ values through the Permian.	167
Fig. 6.9 $\delta^{18}\text{O}_{\text{CO}_3}$ through the Permian-Triassic.	168
Fig. 6.10 $^{87}\text{Sr}/^{86}\text{Sr}$ profile through the Permian.	169

## LIST OF TABLES

## CHAPTER 2

Table 2.0 Basins, sub-basins, wells, and latitudes and longitudes.	23
Table 2.1 Summary of the sections studied.	26
Table 2.2 Bonaparte Basin stratigraphy modified from Mory (1990).	27
Table 2.3 Tern-3. $\delta^{13}\text{C}_{\text{org}}$ , TOC %, and biostratigraphy.	29
Table 2.4 Petrel-4. $\delta^{13}\text{C}_{\text{org}}$ , TOC %, and biostratigraphy.	31
Table 2.5 Fishburn-1. $\delta^{13}\text{C}_{\text{org}}$ , TOC, biostratigraphy.	35
Table 2.6 Sahul Shoals-1 $\delta^{13}\text{C}_{\text{org}}$ , TOC, biostratigraphy.	38
Table 2.7 Canning Basin stratigraphy and depositional environments modified from Middleton (1990).	42
Table 2.8 Paradise Coreholes 1-6, $\delta^{13}\text{C}_{\text{org}}$ , TOC, and biostratigraphy.	45
Table 2.9 Palynology determinations by R. J. Helby (pers. comm. 1993; 1994) of Paradise #4 samples.	47
Table 2.10 Sm/Nd model ages of fine-grained sediments about the $\delta^{13}\text{C}_{\text{org}}$ isotope excursion.	47
Table 2.11 Onslow 1 $\delta^{13}\text{C}_{\text{org}}$ , TOC, biostratigraphy.	51
Table 2.12 Whicher Range-1, $\delta^{13}\text{C}_{\text{org}}$ , TOC, biostratigraphy.	55
Table 2.13 BMR-10 (Beagle Ridge): $\delta^{13}\text{C}_{\text{org}}$ , TOC %, biostratigraphy.	57
Table 2.14 Denison NS 20. $\delta^{13}\text{C}_{\text{org}}$ , TOC, biostratigraphy.	62
Table 2.15 GSQ Eddystone-1. $\delta^{13}\text{C}_{\text{org}}$ , TOC, $\delta^{13}\text{C}_{\text{CO}_3}$ , $\delta^{18}\text{O}_{\text{CO}_3}$ , biostratigraphy and formations.	65
Table 2.16 GSQ Eddystone-5 $\delta^{13}\text{C}_{\text{org}}$ , TOC, $\delta^{13}\text{C}_{\text{CO}_3}$ , $\delta^{18}\text{O}_{\text{CO}_3}$ , cathodoluminescence (C.L.) of carbonate samples, biostratigraphy, and formations.	69
Table 2.17 Taroom-10. $\delta^{13}\text{C}_{\text{org}}$ , TOC, $\delta^{13}\text{C}_{\text{CO}_3}$ , $\delta^{18}\text{O}_{\text{CO}_3}$ , biostratigraphy.	71
Table 2.18 Murrays Run-1. $\delta^{13}\text{C}_{\text{org}}$ , TOC %, H/C, N/C, and biostratigraphy.	76
Table 2.19 Bunnerong DDH 1. $\delta^{13}\text{C}_{\text{org}}$ , TOC % and biostratigraphy.	79
Table 2.20 Lisarow DDH 1. $\delta^{13}\text{C}$ , TOC%, biostratigraphy.	82
Table 2.21 Awaba DDH 2. $\delta^{13}\text{C}$ , TOC, biostratigraphy.	84
Table 2.22 Newvale DDH 28 $\delta^{13}\text{C}_{\text{org}}$ , TOC, biostratigraphy.	86
Table 2.23 Merrimelia-3. $\delta^{13}\text{C}_{\text{org}}$ , TOC, and notes on samples.	92
Table 2.24 Merrimelia-3 palynology	93
Table 2.25 Popotonoa Fm $\delta^{13}\text{C}_{\text{org}}$ , TOC %.	97
Table 2.26 SW1/67, $\delta^{13}\text{C}$ , TOC %, and biostratigraphy (Helby pers. comm., 1994).	99
Table 2.27 CSIRO anthracite standard analyses.	103

## CHAPTER 3

Table 3.1 Sample localities.	106
Table 3.2 Comparison between $\delta^{13}\text{C}_{\text{CO}_3}$ and $\delta^{18}\text{O}_{\text{CO}_3}$ from cathodoluminescent and nonluminescent brachiopod shells.	107
Table 3.3 Strontium isotope results.	111

## CHAPTER 4

Table 4.1 Comparison between $\delta^{13}\text{C}_{\text{CO}_3}$ and $\delta^{18}\text{O}_{\text{CO}_3}$ values obtained from cathodoluminescent and noncathodoluminescent portions of brachiopod or bivalve shells.	120
Table 4.2 Carbonate carbon isotope results.	121
Table 4.3 Oxygen isotope values and estimated temperatures.	129
Table 4.4 Locality of outcrop samples.	130

## CHAPTER 5

Table 5.1 Merrimelia-3 magnetic inclination.	133
--	-----

## CHAPTER 6

Table 6.1 Summary of the key sections.	139
Table 6.2 Carbon isotopes by palynology zone.	141
Table 6.3 Organic carbon burial by palynological stage.	143
Table 6.4 Mass balance constraints.	146
Table 6.5 Carbon reservoirs.	147
Table 6.6 Extinction mechanism evaluation.	151
Table 6.7 Permian- Triassic events.	155
Table 6.8 Strontium isotope values in the Permian.	170

## ABSTRACT

The Permian-Triassic boundary mass extinction is the largest in the Phanerozoic and therefore is the major event in the Phanerozoic. The mass extinction cause is problematical but studying global geochemical and geophysical signatures about the Permian-Triassic boundary can provide insights into the cause of the mass extinction. Global events about the Permian-Triassic boundary are marked by changes in:

- $\delta^{13}\text{C}$  values of carbon
- $^{87}\text{Sr}/^{86}\text{Sr}$  in unaltered marine calcite
- magnetic polarity.

This study aims to identify these features in the sedimentary record and to test the calibration of the Australian biostratigraphical schemes to the global geological timescale.

The following features are found in the Permian-Triassic sediments of Australia:

- a  $\delta^{13}\text{C}_{\text{org}}$  in Total Organic Carbon excursion in 12 marine and nonmarine sections from Northwest to Eastern Australia
- a  $^{87}\text{Sr}/^{86}\text{Sr}$  minimum in a composite section mainly from the Bowen Basin
- a magnetic polarity reversal in the Cooper Basin, central Australia.

The Australian sections are thus time correlated, as follows:

The negative  $\delta^{13}\text{C}_{\text{org}}$  excursion indicates the Permian-Triassic boundary and occurs:

- 1) in Eastern and Central Australia at the change from coal measures to barren measures with red beds at the beginning of the Early Triassic coal gap;
- 2) in Northwest Australia about the boundary between the Hyland Bay Formation and the Mount Goodwin Formation in the Bonaparte Basin and at the boundary between the Hardman Formation and the Blina Shale in the Canning Basin.

The base of the negative  $\delta^{13}\text{C}_{\text{org}}$  excursion lies at or near the base of the *Protohaploxylinus microcorpus* palynological zone.

The  $^{87}\text{Sr}/^{86}\text{Sr}$  minimum determined about the Guadalupian/Ochoan stage boundary in North America is found in the Bowen Basin about the boundary between the Ingelara and Peawaddy Formations.

The  $\delta^{13}\text{C}_{\text{org}}$  excursion in the Cooper Basin is near a magnetic reversal within the Permo-Triassic mixed superchron.

The implications of these findings include:

- confirmation of the traditional placement of the Permian-Triassic boundary at the coal measures/barren measures with redbeds boundary in Eastern Australia
- the linking of the Permian-Triassic boundary to a mass extinction of plant species on land and the beginning of the Triassic coal gap indicated by the *Falcisporites* Superzone base that is coincident with the negative  $\delta^{13}\text{C}_{\text{org}}$  excursion

- a mass extinction causal model that links the  $^{87}\text{Sr}/^{86}\text{Sr}$  minimum determined about the Guadalupian/Ochoan stage boundary to a fall in sealevel that led to changing global environmental conditions. The model invokes greenhouse warming as a contributing cause of the mass extinction.